

Research Paper

Stearoyl-CoA Desaturase-1 dependent lipid droplets accumulation in cancer-associated fibroblasts facilitates the progression of lung cancer

Yana Zhang^{1,2}, Zhuoyu Gu^{1,2}, Jiajia Wan^{1,2}, Xiaohan Lou^{1,2}, Shuangqing Liu^{1,2,3}, Yuan Wang^{1,2}, Yangyang Bian⁴, Fei Wang^{1,2}, Zhenzhen Li^{1,2,✉}, Zhihai Qin^{1,2,3,✉}

1. Medical Research Center, The First Affiliated Hospital of Zhengzhou University, Zhengzhou, Henan 450052, China.

2. Henan International Joint Laboratory of Tumor Immune Microenvironment, Zhengzhou, Henan 450052, China.

3. Key Laboratory of Protein and Peptide Pharmaceuticals, Institute of Biophysics, Chinese Academy of Sciences, Beijing 100101, China.

4. College of Life Science, Northwest University, Xi'an, Shanxi 710069, China.

✉ Corresponding authors: Zhihai Qin, Medical Research Center, The First Affiliated Hospital of Zhengzhou University, Zhengzhou, Henan 450052, China. E-mail: zhihai@ibp.ac.cn; or Zhenzhen Li, Medical Research Center, The First Affiliated Hospital of Zhengzhou University, Zhengzhou, Henan 450052, China. E-mail: lzzkiki@126.com.

© The author(s). This is an open access article distributed under the terms of the Creative Commons Attribution License (<https://creativecommons.org/licenses/by/4.0/>). See <http://ivyspring.com/terms> for full terms and conditions.

Received: 2022.05.09; Accepted: 2022.09.26; Published: 2022.10.18

Abstract

Rationale: Cancer-associated fibroblasts (CAFs) are the main components in the tumor microenvironment (TME) and facilitate lung cancer progression. Studies have reported that metabolic reprogramming can regulate the function of CAFs, especially abnormal lipid metabolism. Lipid droplets (LDs) are ubiquitous organelles that store neutral lipids and have a crucial role in lipid metabolism. However, little is known about the synthesis and functions of LDs in lung CAFs.

Methods: *TetO-EGFR^{L858R}:CCSP-rtTA* transgenic mouse model was used to establish a spontaneous pulmonary tumor model and investigate the accumulation of LDs in CAFs. The effect of LDs accumulation on the phenotype change of fibroblasts was estimated *in vitro* using mouse fibroblast cell lines. RNA sequencing, Western blotting, RT-PCR, and DNA-pull down were performed to determine the mechanism of LDs synthesis in fibroblasts.

Results: We found that LDs were enriched in lung CAFs and induced the pro-tumoral phenotype of CAFs with increased expression of α-smooth muscle actin (α-SMA) and Collagen alpha-2 (I) chain (COL1A2). As the main regulator, hypoxia-inducible factor-1α (HIF-1α) was highly expressed in activated fibroblasts and increased the content of LDs. RNA-sequencing results showed that Stearoyl-CoA Desaturase1 (SCD1) was a downstream gene of HIF-1α, which upregulated the number of LDs in fibroblasts. Importantly, SCD1 inhibition reduced the growth of lung tumors, which was correlated with LDs decrease in CAFs. Analysis of human lung adenocarcinoma tissue chip revealed that CAFs with a high level of SCD1 were positively correlated with the expression of HIF-1α and poor survival in lung cancer patients.

Conclusions: The HIF-1α/SCD1 axis regulates the accumulation of LDs in CAFs, which might represent a novel target for lung cancer therapy.

Key words: Lung Cancer; Cancer-associated Fibroblasts; Lipid Droplets; Hypoxia-Inducible Factor-1α; SCD1

Introduction

The incidence of lung cancer is second only to breast cancer, while it is the leading cause of cancer-related deaths; an estimated 1.8 million deaths were caused by lung cancer in 2020 [1]. Studies have shown that the behavior of cancers is determined by both cancer cells and the tumor microenvironment (TME) [2]. Cancer-associated fibroblasts (CAFs) are one of the most important components of the TME and show

a high expression of several proteins such as α-smooth muscle actin (α-SMA), fibroblast-activating protein (FAP), collagen alpha-2 (I) chain (COL1A2), and podoplanin (PDPN) [3, 4]. Because of the non-specific markers, CAFs comprise many sub-types with different functions [3, 5]. The functions of CAFs are strongly related to the progression of lung cancer [6]. For example, during the progression of lung

cancer, CAFs regulate the synthesis and remodeling of the extracellular matrix and the production of growth factors, which increase the stiffness of tumor tissue and tumor growth [7, 8]. CAFs-mediated paracrine transforming growth factor- β (TGF- β) signaling leads to tumor heterogeneity in lung cancer [9]. Besides, CAFs decrease the chemosensitivity of lung cancer cells by inhibiting cisplatin-induced apoptosis [10]. However, many studies have shown that the functions of CAFs are determined by the different subtypes [11], which makes it challenging to study CAFs.

During tumor progression, the metabolic reprogramming of CAFs not only provides energy for tumor cells, but also improves the survival of themselves in the TME [12]. For example, CAFs can promote cancer progression by secreting growth factors and amino acids [13]. Besides, CAFs release metabolic intermediates such as lactic acid and L-Glutamine, which can be utilized by tumor cells [14, 15]. Many studies have shown that the metabolic reprogramming of CAFs affects the behaviors of tumor cells [16], but how metabolic reprogramming directly influences the function of CAFs is unclear. It is well-known that chronic hypoxia can induce epigenetic reprogramming of glycolysis in fibroblasts to protect them from a poor TME [17]. Lipid metabolism is the main part of metabolism and is essential for the maintenance of the malignant microenvironment [16]. As a part of lipid metabolism, lipid droplets (LDs) are storage organelles at the center of lipid and energy homeostasis and play important roles in regulating the cell phenotypes. Studies have shown that the increased number of LDs is positively correlated with the stemness of breast cancer cells [18]. Besides, sodium oleate induces the accumulation of LDs and regulates the suppressive phenotype of myeloid cells [19]. Inhibiting the formation of LDs causes the transformation of the phenotype of macrophages from M2 to M1 [20]. However, there is no study focusing on the effects of LDs on CAFs in lung cancer.

The synthesis of LDs includes the conversion of excess free fatty acids (FAs) into neutral triglycerides (TAGs) and their storage in LDs, which can serve as the main source of energy [21, 22]. The regulation of FA uptake, synthesis, storage, and usage depends on hypoxia-inducible factor-1 α (HIF-1 α) [23]. HIF-1 α -mediated metabolic reprogramming is involved in a variety of tumor processes including lung cancer progression [24, 25]. The complex environment in tumors also influences the expression of HIF-1 α in a variety of stromal cells in the TME [24, 26]. Our previous study demonstrated that hypoxia, TGF- β 1, and tumor conditioned medium (CM) increase the

expression of HIF-1 α , which plays an important role in the activation of CAFs [8]. However, little is known about the connection between HIF-1 α and the accumulation of LDs in CAFs.

Here, we identified HIF-1 α as a novel SCD1 promoter-binding protein that promotes the accumulation of LDs in fibroblasts. Additionally, the high content of LDs induces the upregulation of α -SMA and COL1A2, which in turn activate fibroblasts. Targeting the HIF-1 α /SCD1 axis in CAFs might be a promising strategy for lung cancer therapy.

Methods

Tumor models and treatments

All mice were kept in specific pathogen-free conditions and conducted with approval from the First Affiliated Hospital of Zhengzhou University Ethics Committee. The transgenic mice (*TetO-EGFR^{L858R}; CCSP-rtTA*) were obtained from Professor Lin Xin of Tsinghua University and described previously [27]. To induce the growth of lung tumors, doxycycline (1 mg/mL) was administered to the mice through drinking water at five weeks of age. The water was changed every two days for 3.5 months. After the mouse lung cancer model was established, the SCD1 inhibitor A939572 (20 mg/kg) or vehicle was administered through oral gavage daily for 14 days.

For mice experiments, Mouse Lewis lung cancer (LLC) cells (1×10^5 /mouse) were co-injected with or without fibroblasts (1×10^6 /mouse; NIH 3T3 or MEF) subcutaneously into C57 mice (Beijing Charles River Laboratory Animal Company). From the eighth day, tumor growth was monitored every two days, and tumor volume was calculated as length \times width \times width/2.

Cells isolation and culture

Mouse Lewis lung cancer (LLC) cells were obtained from Professor Li Yan of the Academy of Military Medical Sciences. MEF cells (immortalized MEF cells) were a gift from Prof. Lin Xin of Tsinghua University. The NIH 3T3 cell line was obtained from ATCC (Manassas, VA, USA) and cultured with Dulbecco's modified eagle medium (DMEM) containing 10% fetal bovine serum (FBS, ST30-3302, PAN-Biotech GmbH). The LLCs were transfected with a lentivirus green fluorescence protein (GFP) according to previously described method [28]. Mouse primary lung CAFs and normal fibroblasts (NFs) were isolated from the mouse lung cancer model (*TetO-EGFR^{L858R}; CCSP-rtTA*) as previously described [8]. The cultured CAFs and matched NFs were used after five passages following primary culture. After 72 h of incubation, the conditioned

medium of the LLC cells (CM) was collected and centrifuged at 16,000 g for 5 min to remove cell debris. The cells were cultured at 37 °C, 5% CO₂, and 20% O₂, except for those with special instructions. The hypoxic condition was 37 °C, 1% O₂, 5% CO₂, and 94% N₂.

H&E staining and Masson staining

The tissue sections were deparaffined and rehydrated as described previously [29]. After routine processing, lung tissue sections (6 μm thick) were stained with H&E for histological analysis and Masson staining for collagen deposition analysis.

Oil Red O Staining

Frozen sections from mice subcutaneous tumors and the slides with cells were fixed in 4% formalin for 20 min, then washed with 60% propylene glycerol. The sections were stained with 0.5% Oil Red O (Sigma, St. Louis, Missouri, USA) in propylene glycerol for 10 min at 60 °C, and the cells were stained for 5 min at room temperature. Nuclei were counterstained with hematoxylin for bright-field microscopic examination. The red LDs were visualized by microscopy, and the fluorescence intensity was analyzed by using Image J.

Tissue and cell immunofluorescence

OCT-embedded samples were sectioned, and the frozen slides or cells were fixed with 4.0% paraformaldehyde and incubated for 15 min at room temperature. The sections were blocked with 5% bovine serum albumin in PBST (tween-20) and incubated with primary antibodies overnight at 4 °C. The primary antibodies used included goat anti-α-SMA (Abcam, Cat# Ab21027), rabbit anti-s100a4 (Abcam, Cat# Ab27957), rabbit anti-ADRP (Proteintech, Cat#15294-I-AP) and rabbit anti-Proliferating cell nuclear antigen (PCNA) (Proteintech, Cat#10205-I-AP). The slides were incubated with the immunofluorescent secondary antibody for 0.5 h at room temperature in the dark. A tissue microarray (HLugA180Su07) was purchased from Shanghai Outdo Biotech Company. For the tissue microarray, it was de-waxed and heat-induced for antigen retrieval. The tissue microarray was incubated with anti-α-SMA (CST, Cat# 56856S), anti-HIF-1α (Abcam, Cat# ab179483) and anti-SCD1 (CST, Cat# 2794S); the PPD-540 and PPD-620 digital image system (PANOVUE, China) were used for visualization. The nuclei were stained using Fluoro-Gel II 20 with DAPI (Electron Microscopy Sciences, USA), and the slides were examined by fluorescence microscopy.

Flow cytometry sorting

Single-cell suspensions prepared directly from

lung cancer tissues and normal lung tissues were stained with PE-labelled anti-EpCAM (clone G8.8), APC-labelled anti-CD31 (clone MEC13.3), and Alexa Fluor 700-labelled anti-CD45 (clone I3/2.3). The dead cells were labelled with DAPI, and the LDs were labelled with BODIPY®493/503. All antibodies were purchased from Biolegend (California, USA). The cells were analyzed using FACSCanto II (BD Biosciences, San Diego, USA).

Materials and reagents

Cobalt chloride (Cocl2) and PF-06424439 (inhibitor of DGAT2) were obtained from Sigma-Aldrich. BODIPY®493/503, LipidTOX™ neutral lipid stain, and Lipofectamine 3000 were purchased from Invitrogen (California, USA). TGF-β1 was obtained from Pepro Tech (Rocky Hill, USA). The inhibitors A939572 (inhibitor of SCD1), A922500 (inhibitor of DGAT1), and JZL-184 (inhibitor of MAGL) were obtained from MedChemExpress (New Jersey, USA).

BODIPY®493/503 Staining

Cells were washed with PBS and labeled with BODIPY®493/503 at 37 °C for 15 min. Then, the cells were digested and analyzed using the FACS Canto II device (BD Biosciences).

HCS LipidTOX™ neutral lipid stains

Cells were fixed with 4.0% formaldehyde and incubated for 30 min. Formaldehyde was removed, and then the cells were labeled with the neutral lipid staining solution. The 1,000× LipidTOX™ neutral lipid stain (Invitrogen) was diluted 1:1,000. The plates were sealed at room temperature for 30 min before imaging.

Real-time quantitative polymerase chain reaction (RT-qPCR)

Total RNA was extracted using RNAiso plus (TAKARA; #1089527), according to a previously described protocol, and reverse transcribed using PrimeScript RT reagent kit with gDNA Eraser (TAKARA; #RR047A). Real-time qPCR was performed using SYBR GreenTM Primix Ex TaqTM II (TAKARA; #RR820A) in Step One® sequence detection system (Applied Biosystems, Milan, Italy). Each sample was examined at least in triplicate. The relative RNA expression was calculated using the $2^{-\Delta\Delta Ct}$ method. The primers used are presented in the supplementary data (Table S1). The gene of the ribosomal protein 18S was used as a control gene to obtain normalized values.

Western blot analysis

The cultured cells were lysed in RIPA buffer with 1% PMSF, 2% protease, and phosphatase

inhibitors for 30 min, and the protein concentrations were measured with the BCA kit. The lysates were fractionated by 10% SDS-PAGE and transferred onto a nitrocellulose membrane. The following primary antibodies were used: anti- α -SMA (Abcam, ab21027; diluted 1:1,000), anti-COL1A2 (ProteinTech; 14695-I-AP; diluted 1:200), anti-HIF-1 α (R&D Systems; Mab1536; diluted 1:1,000), anti-SCD1 (Origene, TA309938; diluted 1:1,000), and anti- β -Actin (Abclonal, AC006; diluted 1:10,000). Thereafter, the membranes were incubated with the corresponding secondary Horseradish-peroxidase-conjugated (HRP) conjugated antibodies. The signals were detected using the western ECL substrate (ConWin Biotech, Beijing, China).

Adenovirus Construction, Purification, and Infection

The HIF-1 α (NM_001313919.1) knockout fibroblasts (NIH 3T3 and MEF cells) were constructed and stored in our laboratory as described previously [8]. SCD1-overexpressed (NM_009127.4) lentiviral fluid was purchased from Genechem Company (Shanghai). Cells were transfected with the lentiviral fluid, and the stable clones were selected after two weeks using 3 μ g/mL puromycin.

RNA-sequencing analysis

The expression of HIF-1 α was knocked out in NIH 3T3 by CRISPR Cas9 as indicated before [8]. Total RNA was extracted by using Trizol (Invitrogen, Carlsbad, CA, USA) and subjected to RNA-sequencing analysis by Beijing Genomics institution (BGI, Shenzhen, China). The raw transcriptomic reads were mapped to a reference genome and the gene expression levels by using BGI Dr.Tom 3.0. Significantly differentially expressed genes were acquired by setting log 2fold change >0.0 .

Promoter reporters and Dual-luciferase assay

A fragment containing the core promoter region of mSCD1 was inserted between the xHOI and kpnI sites of the firefly luciferase vector pGL4.10, and the Renilla luciferase control reporter vector pRL-TK was used as a control. The cells (2×10^4 cells/well) were seeded in a 96-well plate. After the cell confluence reached 70%, pGL4.10-hTERT-85 and pRL-TK were transfected into 3T3-MOCK and 3T3-OVER cells with Lipofectamine 3000 (Invitrogen, Carlsbad, CA). Dual-luciferase assay was performed using the Dual-Luciferase® Reporter Assay System (Promega, Madison, WI).

Streptavidin-agarose pulldown assay

The mSCD1 promoter-binding proteins were analyzed by the streptavidin-agarose pulldown assay

as described previously [30]. Briefly, nuclear protein extracted from NIH 3T3 cells was incubated with 10 μ g of biotin-labeled double-stranded DNA probes corresponding to the nucleotide -85 to +197 of the mSCD1 promoter region and 100 μ L of streptavidin-agarose beads at 4 °C overnight. The mixture was then centrifuged at 500 g. The DNA-protein complex was fractionated by 10% SDS-PAGE and incubated with an anti-HIF-1 α primary antibody. The bound proteins were visualized by the western ECL substrate.

Data analysis

All data are presented as the Mean \pm SD using GraphPad Prism V 7.0. Comparisons between two groups were calculated using unpaired Student's t test and comparisons of more than two groups were determined using one-way ANOVA Tukey's multiple comparisons. The survival analysis was determined by the Kaplan-Meier plotter. Differences between groups with p-values lesser than 0.05 were considered to be statistically significant.

Results

Accumulation of LDs in lung CAFs

The mouse lung cancer model (*TetO-EGFR^{L858R}; CCSP-rtTA*) was established using doxycycline hydrochloride (Figure 1A) [31]. The results of H&E staining showed that the normal lung epithelial cells were replaced by a jumble of tumor cells with hyperchromatic nuclei. Besides, there was more collagen deposition and accumulation of LDs in the lung cancer tissues compared to that in the normal lung tissues, as demonstrated by Masson and Oil Red O staining (Figure 1B). Adipose differentiation-related protein (ADRP) is an LD protein found in most cells and tissues [19]. By co-staining ADRP and α -SMA, we found that lung CAFs were enriched with LDs (Figure 1C). Additionally, CAFs and NFs (DAPI-/CD45-/CD31-/EPCAM $^+$ cells) were analyzed by flow cytometry to confirm the higher enrichment of LDs in CAFs (Figure 1D).

To further confirm the above findings, the primary CAFs and NFs were isolated and cultured *in vitro* (Figure 1E). CAFs were identified with higher expression of α -SMA and S100A4 compared to their expression in NFs (Figures S1A and S1B), which was similar to the results found in other studies [3]. Oil Red O staining revealed that more LDs were also observed in cultured CAFs compared to that in NFs (Figure 1F). These findings suggested that the accumulation of LDs might be one of the characteristics of CAFs, which is independent of the *in vivo* or *in vitro* environment.

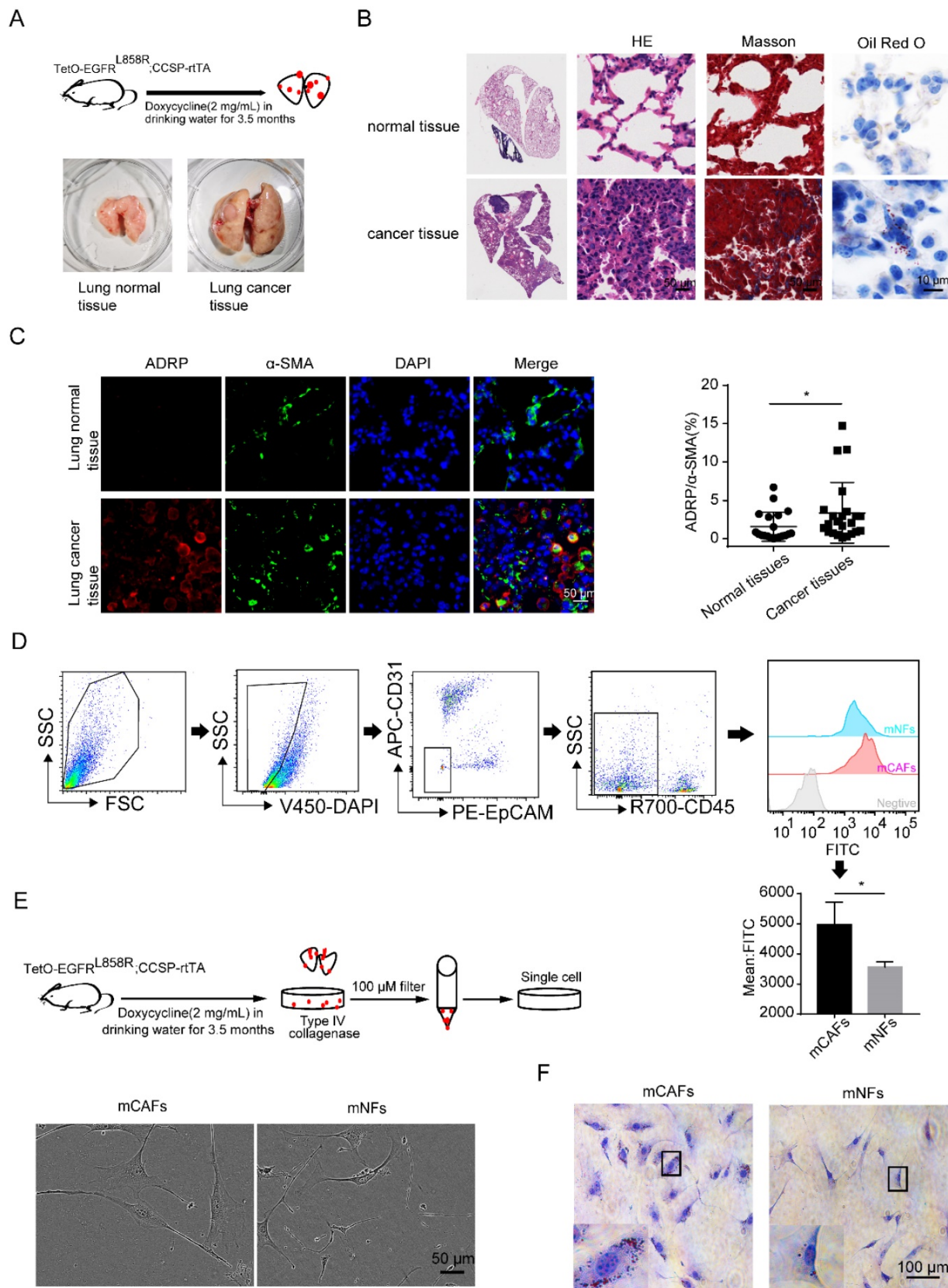


Figure 1. Accumulation of LDs in lung CAFs. **(A)** The doxycycline-induced mouse lung cancer model (TetO-EGFR^{L858R}; CCSP-rtTA) was established (N = 5). **(B)** Representative images of mouse lung cancer tissues and normal lung tissues after H&E staining, Masson staining and Oil Red O staining (Scale bar of H&E and Masson: 50 μ m; Scale bar of oil red O: 10 μ m). **(C)** Representative immunofluorescence images of ADRP (red) co-stained with α -SMA (green) in frozen sections of mouse lung cancer tissues and normal lung tissues (DAPI: blue; Scale bar: 50 μ m). **(D)** The LD contents of CAFs and NFs (DAPI/CD45-/CD31-/EpCAM-) were detected by BODIPY staining (FITC) (N = 5). **(E)** The morphology of mCAF and mNF isolated from doxycycline-induced mouse lung cancer model (TetO-EGFR^{L858R}; CCSP-rtTA) under white light (Scale bar: 50 μ m, N = 3). **(F)** The Oil Red O staining of mCAF and mNF (Scale bar: 100 μ m). Data are shown as the Mean \pm SD; *p < 0.05.

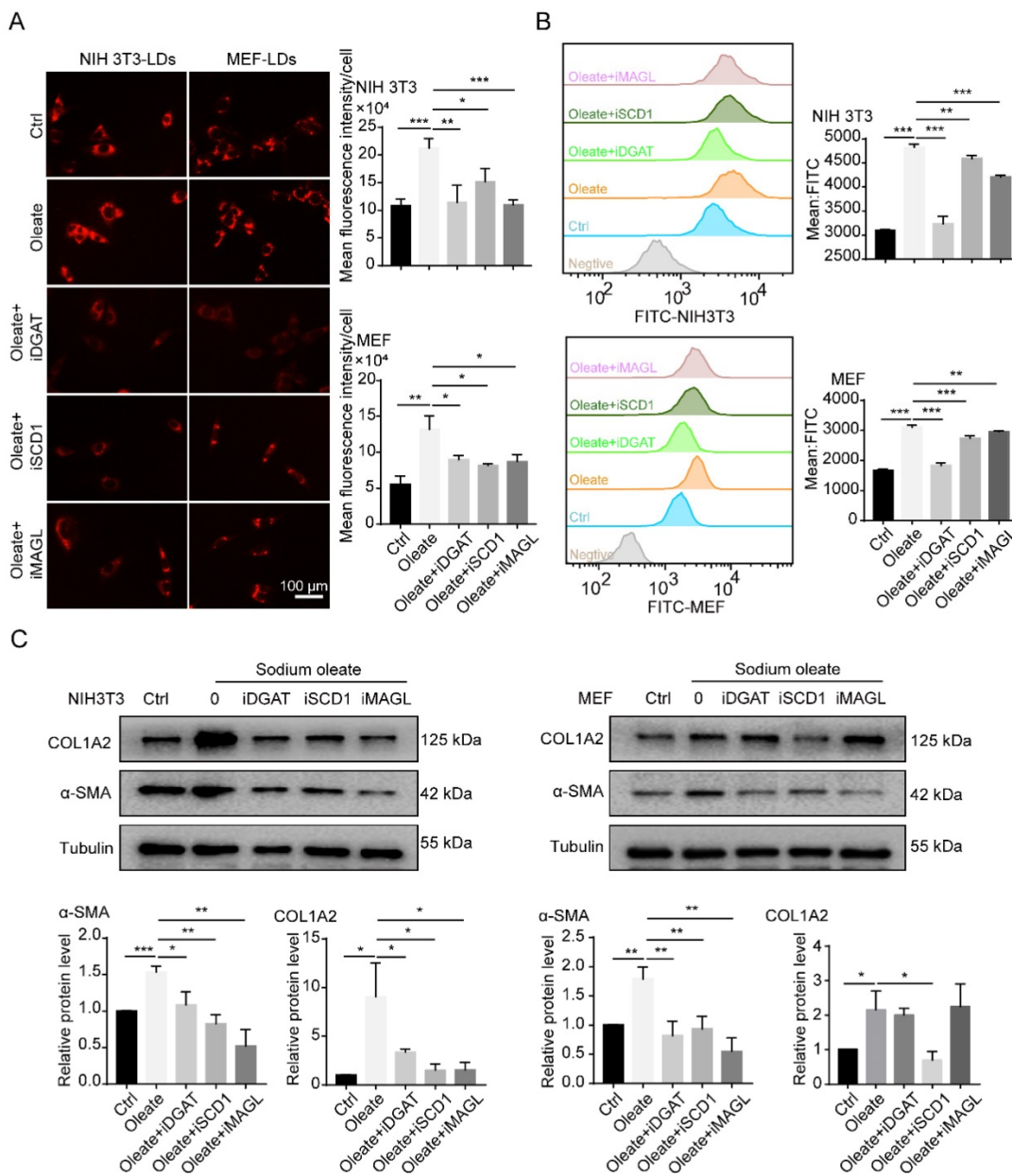


Figure 2. The accumulation of LDs is involved in the regulation of fibroblast activation. (A) The lipid-tox red staining of fibroblasts (NIH 3T3 and MEF) that were treated with/without sodium oleate (50 μ M) and the LDs inhibitors (iDGAT: iDGAT1-10 μ M+ iDGAT2-10 μ M, iSCD1-100 nM, iMAGL-20 nM; Scale bar: 100 μ m) for 12h (N = 5). (B) The BODIPY staining (FITC) of fibroblasts (NIH 3T3 and MEF) that were treated with/without sodium oleate (50 μ M) and the LDs inhibitors (iDGAT, iSCD1 and iMAGL) for 12h (N = 3). (C) The protein expression of α -SMA and COL1A2 in fibroblasts (NIH 3T3 and MEF) that were treated with/without sodium oleate (50 μ M) and the LDs inhibitors (iDGAT, iSCD1 and iMAGL) for 24h (N = 3). Data are shown as the Mean \pm SD; *p < 0.05, **p < 0.01, ***p < 0.001.

The accumulation of LDs is involved in the regulation of fibroblast activation

CAFs are considered to be the activated fibroblasts in the TME [2]. To further understand the effect of LDs on CAFs, we investigated the relationship between the accumulation of LDs and fibroblast activation. Sodium oleate was reported to induce lipid synthesis in cultured fibroblasts [19]. In line with expectations, sodium oleate significantly upregulated the number of LDs in fibroblasts and increased the expression of COL1A2 and α -SMA (Figures 2A-2C). During the formation of LDs, SCD1

is responsible for the synthesis of unsaturated fatty acids, including palmitoleic (C16:1 n-7) and oleic (C18:1 n-9) acids, while diglyceride acyltransferase (DGAT) controls the transformation of free FAs into LDs and monoacylglycerol lipase (MAGL) mainly plays an important role in the export of LDs into the cytoplasm [19]. When the catalytic activities of SCD1, DGAT and MAGL were blocked, the synthesis of LDs was inhibited in fibroblasts (Figures 2A and 2B), along with the expression of α -SMA (Figure 2C). These results indicated that the accumulation of LDs might regulate the activation of fibroblasts.

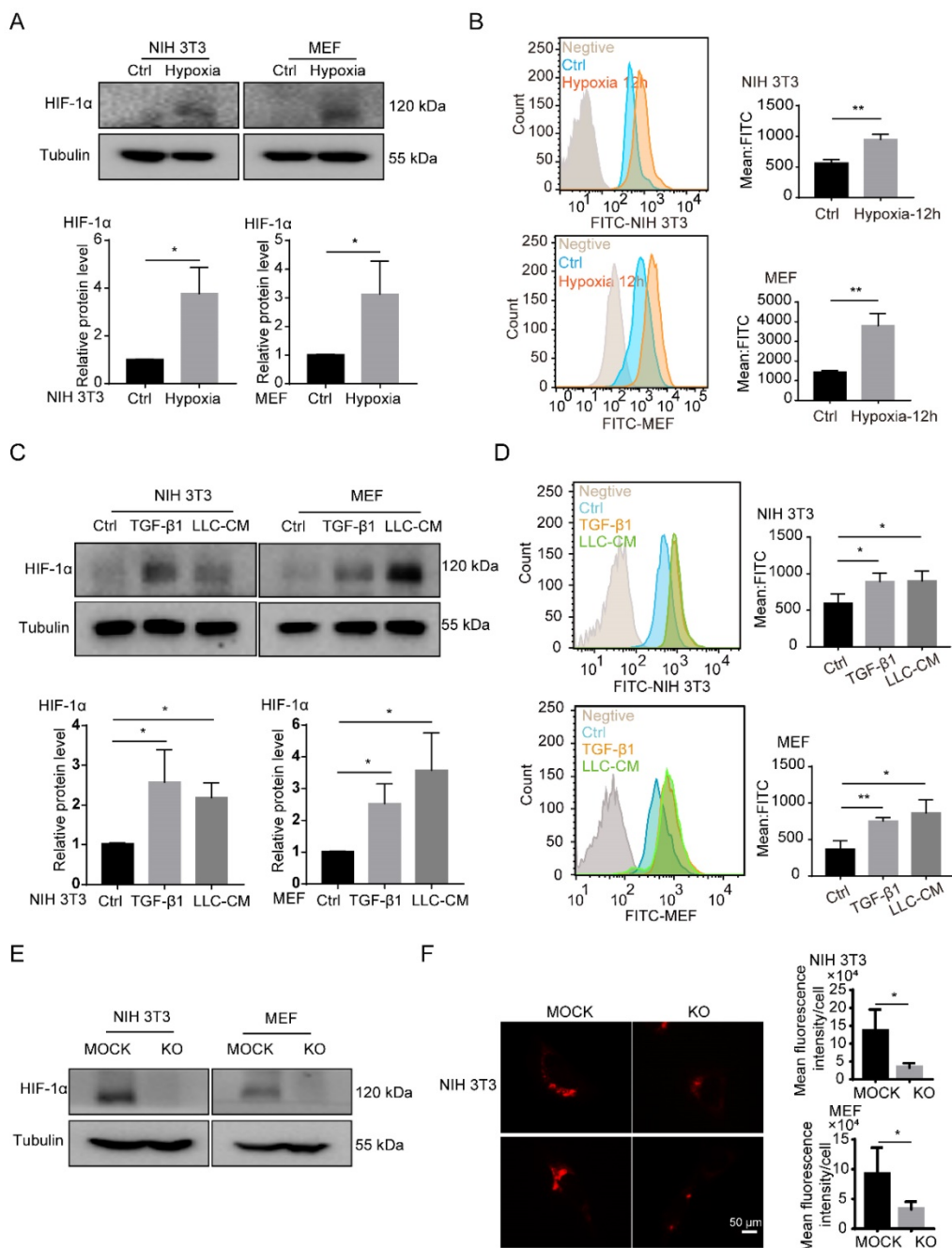


Figure 3. HIF-1 α is necessary for the accumulation of LDs in fibroblasts. **(A)** The protein expression of HIF-1 α in NIH 3T3 and MEF cells under hypoxia treatment (1% O₂; N = 3). **(B)** The BODIPY staining of LDs in fibroblasts (NIH 3T3 and MEF cells) which were treated with hypoxia (1% O₂) for 12 h (N = 3). **(C)** The protein expressions of HIF-1 α in NIH 3T3 and MEF cells treated with TGF- β 1 (2 ng/mL) and LLC conditioned medium (LLC-CM). **(D)** The BODIPY staining of the LDs in the fibroblasts (NIH 3T3 and MEF cells) which were treated with TGF- β 1 and LLC-CM (N = 3). **(E)** The protein expressions of HIF-1 α were detected in HIF-1 α stably knocked out (KO) fibroblasts (NIH 3T3 and MEF cells; N = 3). **(F)** The lipid-tox red staining of the LDs in the HIF-1 α MOCK cells (MOCK) and HIF-1 α KO cells (KO) (NIH 3T3 and MEF cells; Scale bar: 50 μ m; N = 3). Data are shown as the Mean \pm SD; *p < 0.05, **p < 0.01, ***p < 0.001.

HIF-1 α is necessary for the accumulation of LDs in fibroblasts

Consistent with the previous data [8], we found that hypoxia, TGF- β 1 and tumor CM induced the upregulation of HIF-1 α in fibroblasts and the HIF-1 α high-expressed fibroblasts was considered as the CAFs (Figures 3A and 3C). Interestingly, a large number of LDs accumulated in activated fibroblasts,

which were induced by hypoxia, TGF- β 1 and tumor CM (Figures 3B and 3D). Next, to confirm the role of HIF-1 α in the accumulation of LDs in fibroblasts, HIF-1 α was knocked out (KO) in fibroblasts (NIH 3T3 and MEF cells) (Figures 3E). We observed that HIF-1 α deficiency led to an impaired accumulation of LDs in fibroblasts (Figure 3F). These findings suggested that HIF-1 α is essential for the accumulation of LDs in fibroblasts.

HIF-1 α promotes the accumulation of LDs in fibroblasts through SCD1

To determine the mechanisms underlying HIF-1 α -induced accumulation of LDs in fibroblasts, RNA-sequencing analysis was conducted. The volcano plot showed that 2,978 upregulated genes and 3,389 downregulated genes were differentially detected in HIF-1 α -KO fibroblasts (Figure 4A). Most of these genes are related to metabolism, especially involved in lipid synthesis and lipid catabolism (Figures S2A-B and 4B). Then, we performed real-time PCR to validate the characteristic genes. Among these genes, SCD1 was significantly downregulated in NIH 3T3 HIF-1 α -KO and MEF HIF-1 α -KO cells, while other lipid catabolism genes like Acadm and Cpt-1 α were decreased in MEF HIF-1 α -KO fibroblasts but not in NIH 3T3 HIF-1 α -KO fibroblasts (Figures 4C and S2C). We also observed that the expression of SCD1 was promoted by hypoxia, TGF- β 1 and tumor CM (Figures 4D-E, S2D-E). Moreover, decreased SCD1 in HIF-1 α KO cells was reversed by the overexpression of SCD1 through vector transfection in fibroblasts (Figures 4F and S2F).

To explore the mechanism of HIF-1 α in the expression of SCD1, eight oligonucleotide probes with different lengths in the promoter region of SCD1 were designed (Figure S2G). Those probes were used to investigate the effect of HIF-1 α on the SCD1 promoter activity. The luciferase reporter assay showed that KO of HIF-1 α significantly decreased the SCD1 promoter activity of NIH 3T3 cells in the promoter region of -1288 ~ +197 bp, -1129 ~ +197 bp, -931 ~ +197 bp and -85 ~ +197 bp (Figure 4G). Next, the activity of the four promoter regions was further examined. In HIF-1 α KO fibroblasts, SCD1 promoter activity was obviously inhibited in the promoter region of -1129 ~ +197 bp, -931 ~ +197 bp and -85 ~ +197 bp (Figure S2H). As the promoter region of -85 ~ +197 bp was closer to the transcription initiation site, we speculated that HIF-1 α might bind to the DNA region. According to the JASPAR database analysis, we predicted that the binding site of the -85 ~ +197 bp region was the most credible promoter binding site and the binding site sequence of SCD1 was 5'-ACGCCT-3'. To ascertain the binding between HIF-1 α and the SCD1 promoter, a 5'-biotin-labeled DNA probe for the region of -85 ~ +197 bp of the SCD1 promoter was synthesized, the nuclear protein/DNA complex in NIH3T3 cells was detected using synthesized DNA probe or nonspecific probe (NSP) and their binding was validated by western blot analysis (Figure 4H). These results suggested that HIF-1 α can upregulate the expression of SCD1 by regulating the SCD1 promoter activity.

To further investigate the function of SCD1 in

fibroblasts, we established stable SCD1-overexpressing cells (NIH 3T3) (Figures 4I and 4J). BODIPY staining showed that more LDs were found in the SCD1-overexpressing cells (Figures 4K and S2K) and the MEF cells overexpressing SCD1 (Figures S2I and S2J). To confirm the relationship between HIF-1 α and SCD1 in the accumulation of LDs in fibroblasts, we detected the LDs in fibroblasts with or without SCD1 overexpression under hypoxia and found that SCD1-mock and SCD1-overexpression fibroblasts had increased LDs under hypoxia (Figure S2L). These results indicated that SCD1 is the key downstream gene of HIF-1 α that catabolizes the synthesis of LDs in fibroblasts.

SCD1-overexpressing fibroblasts promote lung cancer growth

SCD1, also known as 9-fatty acyl-CoA desaturase, is an endoplasmic reticulum-associated enzyme that catalyzes palmitoyl-CoA and stearoyl-CoA to produce palmitoleic acid (16:1 n-7) and oleic acid (18:1 n-9), which are the main composition of LDs [32]. Next, we investigated whether the accumulation of LDs in fibroblasts could affect tumor growth. For this, we established a co-culture system *in vitro*. After co-cultured with tumor cells, fibroblasts overexpressing SCD1 could increase the accumulation of LDs in tumor cells (Figures 5A and S3B). LDs are imported into cells mainly through fatty acid translocase, also known as CD36 [33]. We found that CD36 expression in tumor cells did not change after they were co-cultured with fibroblasts (Figures 5B and S3D). Interestingly, SCD1-overexpressing fibroblasts localized closer to tumor cells compared with SCD1-mock fibroblasts (Figures 5C and S3C). To further demonstrate whether the increased LDs in SCD1-overexpressing fibroblasts could facilitate lung cancer growth *in vivo*, we established mouse subcutaneous lung cancer models in C57 WT mice. LLC cells were co-injected with or without SCD1-overexpressing fibroblasts subcutaneously into the mice. To eliminate the influence of fibroblasts proliferation on tumor growth, we tested the proliferation of different fibroblasts and found that there was no significant difference between SCD1-mock fibroblasts and SCD1-overexpressing fibroblasts (Figure S3A). However, LLC cells (1×10^5 cells) were co-injected with fibroblasts and tumor growth was monitored for 20 days, we found that the tumor co-injected with fibroblasts form the subcutaneous graft tumor and tumor co-injected with the SCD1-overexpressing fibroblasts grew faster (Figures 5D and S3E). Additionally, tumor weights increased significantly when SCD1-overexpressing fibroblasts co-injected with LLC cells (Figures 5E and S3F).

Furthermore, more PCNA positive cells in the tumor tissues were found when co-injected with SCD1-overexpressing fibroblasts (Figure 5F). These results indicated that the increased accumulation of LDs in fibroblasts promotes lung cancer growth.

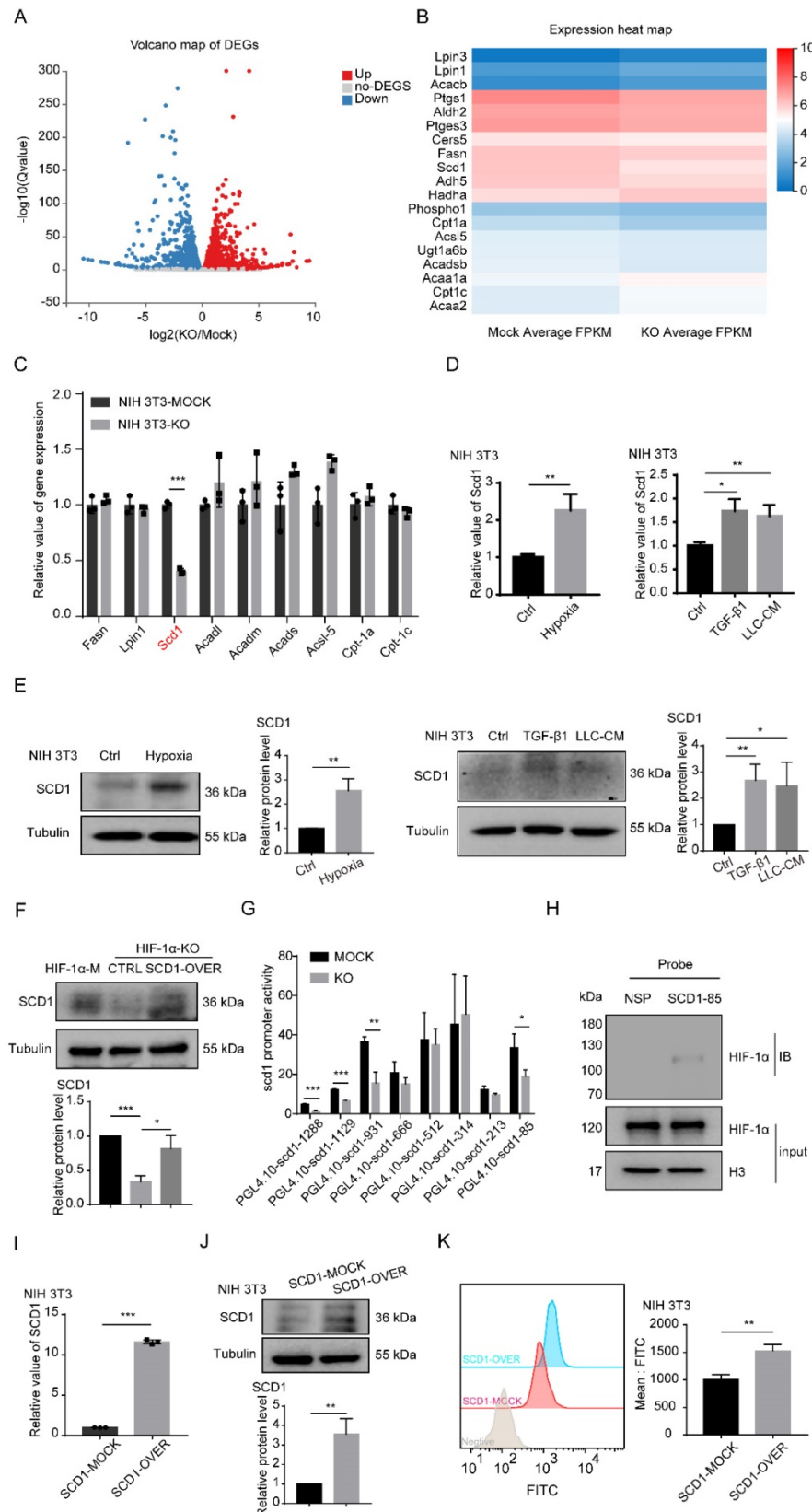


Figure 4. HIF-1α promotes the accumulation of LDs through SCD1. (A) The volcano map of gene changes in fibroblasts (NIH 3T3-HIF-1α-MOCK and NIH 3T3-HIF-1α-KO) by RNA-seq. (B and C) Signature genes involved in lipid metabolism were listed and validated by RT-PCR in fibroblasts (NIH 3T3-HIF-1α-MOCK and NIH

3T-HIF-1 α -KO) (N = 3). (**D and E**) The RNA and protein levels of SCD1 in fibroblasts (NIH 3T3) that were treated with hypoxia (1% O₂), TGF- β 1 and LLC-CM. (**F**) The protein expression of SCD1 in fibroblasts (NIH 3T3-HIF-1 α -MOCK and NIH 3T3-HIF-1 α -KO cells) transfected with the SCD1-overexpression plasmid. (**G**) The relative promoter activity of mSCD1 in NIH 3T3-MOCK and NIH 3T3-KO cells. (**H**) The expression of bound proteins of HIF-1 α in 5'-biotin labeled probes corresponding to the S85 fragment of mSCD1 promoter or a nonspecific probe (NSP) that was incubated with NIH 3T3 cell lysates and streptavidin beads. (**I and J**) The relative expressions of the RNA and protein of SCD1 were determined in the SCD1-MOCK and SCD1-OVER cells (NIH 3T3) (N = 3). (**K**) The BODIPY staining of the LDs in the SCD1-MOCK cells and SCD1-OVER cells (NIH 3T3). Data are shown as the Mean \pm SD; *p < 0.05, **p < 0.01, ***p < 0.001.

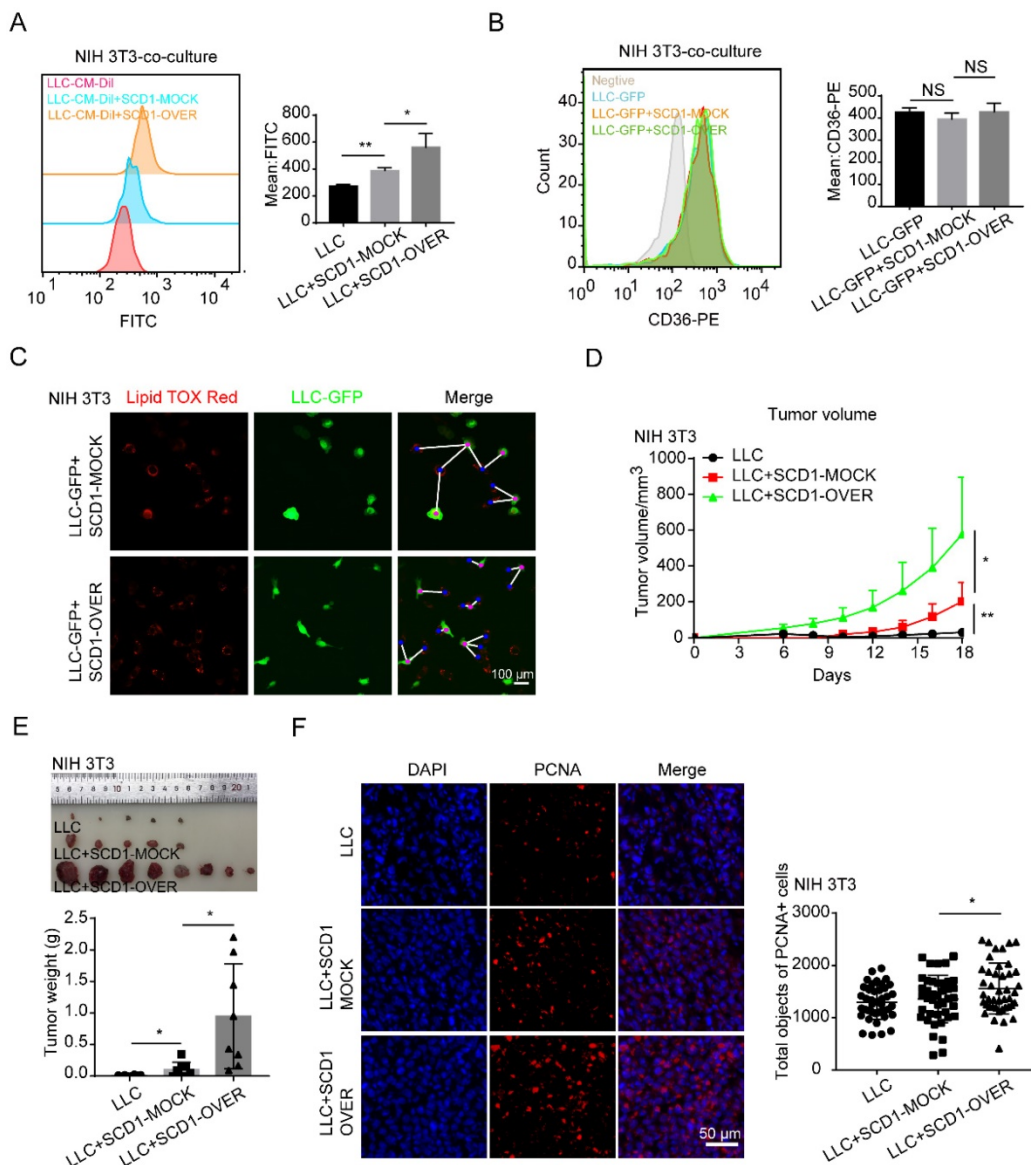


Figure 5. SCD1-overexpressing fibroblasts promote lung cancer growth. (**A and B**) The BODIPY staining and CD36 expression of tumor cells (LLC cells) after co-cultured with or without NIH 3T3-SCD1-MOCK cells and NIH 3T3-SCD1-OVER cells (N = 5). (**C**) The distribution and LD contents of tumor cells (LLC-GFP cells) that were co-cultured with SCD1-MOCK and SCD1-OVER fibroblasts (NIH 3T3) by lipid-tox red staining (Scale bar: 50 μ m, N = 3). (**D**) The LLC cells with or without NIH 3T3-SCD1-MOCK cells or NIH 3T3-SCD1-OVER cells were subcutaneously co-injected into the C57 mice (N = 8 mice/group) and the tumor volumes were measured every two days. (**E**) The representative tumor images and tumor weights are presented. (**F**) Representative immunofluorescence images of PCNA (red) in the frozen sections from the tumor tissues (Scale bar: 50 μ m). Data are shown as the Mean \pm SD; NS: p \geq 0.05, *p < 0.05, **p < 0.01.

SCD1 blockage inhibits lung cancer progression *in vivo*

To monitor the anti-tumor effect of SCD1 inhibitors (iSCD1-A939572) *in vivo*, lung tumor-bearing mice (TetO-EGFR^{L858R}; CCSP-rtTA) were treated with vehicle or A939572 starting at 3.5 months after doxycycline was administered (Figure 6A). Remarkably, iSCD1 treatment profoundly impaired doxycycline-induced lung tumor growth, which also

contained less collagen in lung cancer tissues (Figures 6B and 6C). Additionally, iSCD1 treatment specifically reduced the accumulation of LDs in CAFs, and α -SMA was also downregulated after the administration of iSCD1 (Figure 6D). These results indicated that the SCD1 might be a novel target involved in the accumulation of LDs in fibroblasts, and targeting SCD1 might be a promising therapeutic strategy to inhibit lung cancer growth.

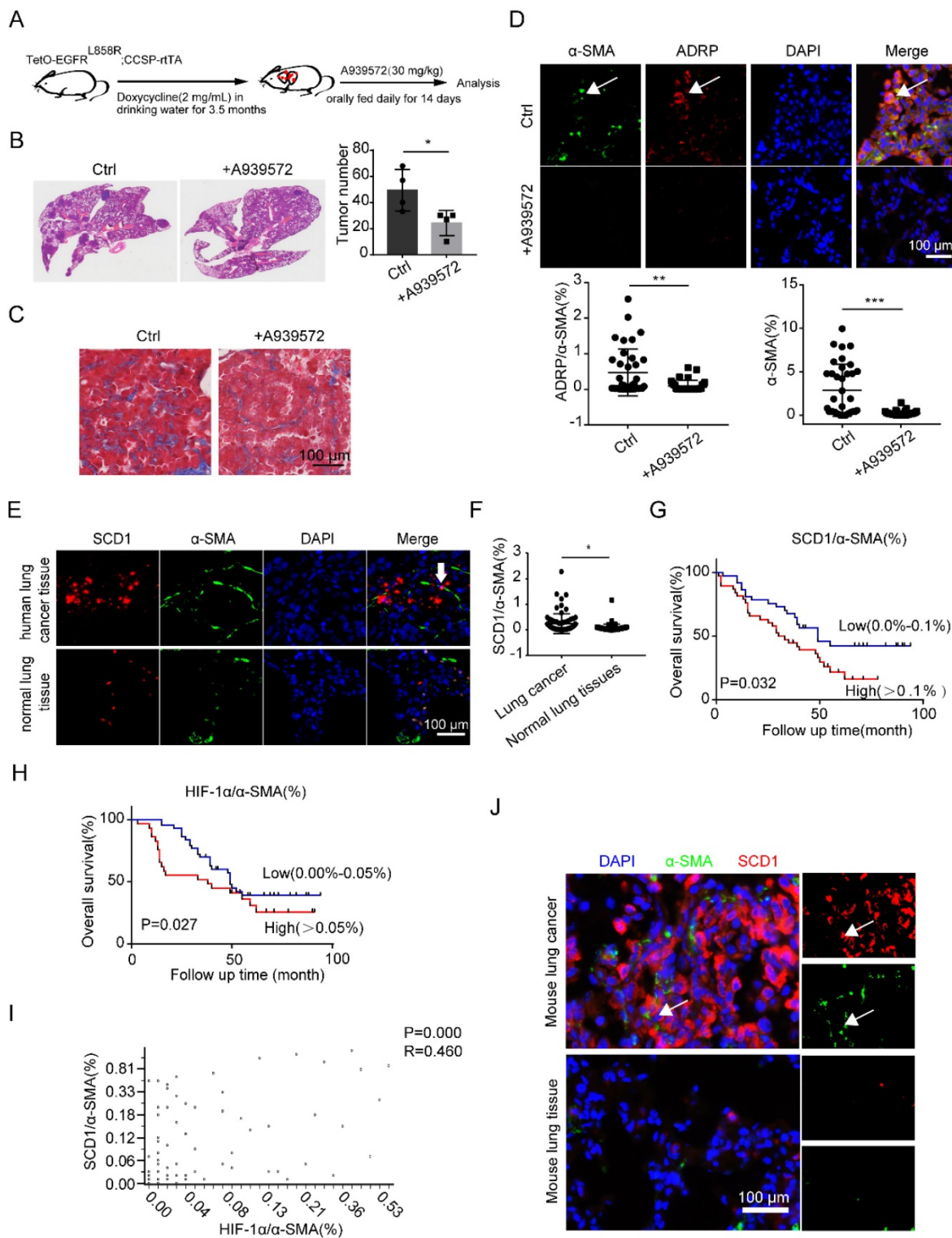


Figure 6. SCD1 blockage inhibits lung cancer progression in vivo. (A) The procedure of doxycycline-induced mouse lung cancer model (*TetO-EGFR^{L858R}; CCSP-rTA*) treated with A939572 (SCD1 inhibitor: 30 mg/kg) daily for 14 days (N = 4 mice/group). (B and C) The H&E and Masson staining of doxycycline-induced mouse lung cancer tissues (*TetO-EGFR^{L858R}; CCSP-rTA*) that were administrated with or without A939572. (D) Representative immunofluorescence images of ADRP (red) co-stained with α-SMA (green) in frozen sections of mouse lung cancer tissues (Scale bar: 100 μm). (E) Representative immunofluorescence images of SCD1 (red) and α-SMA (green) in the lung adenocarcinoma tissue microarray (Scale bar: 100 μm). (F) The statistical analysis of SCD1/α-SMA% expression in lung cancer tissues and normal lung tissues from lung adenocarcinoma tissue microarray data (n = 75). (G) Kaplan-Meier overall survival curves for lung adenocarcinoma patients with low (blue line) or high (red line) expression of SCD1 in fibroblasts (co-staining of SCD1 and α-SMA). “Low” indicates that the percentage of co-staining of SCD1 and α-SMA cells is 0.0%-0.1% and “high” indicates the percentage of co-staining of SCD1 and α-SMA cells is > 0.1%. (H) Kaplan-Meier overall survival curves for lung adenocarcinoma patients with low (blue line) or high (red line) expression of HIF-1α in fibroblasts (co-staining of HIF-1α and α-SMA). “Low” indicates that the percentage of co-staining of HIF-1α and α-SMA cells is 0.0%-0.05% and “high” indicates that the percentage of co-staining of HIF-1α and α-SMA cells is > 0.05%. (I) Correlation analysis of co-staining of SCD1 and α-SMA and co-staining of HIF-1α and α-SMA in lung adenocarcinoma paraffin section samples from lung adenocarcinoma tissue microarray (Pearson’s correlation test, n = 68, r = 0.460, p = 0.000). (J) Representative immunofluorescence images of SCD1 (red) co-stained with α-SMA (green) in frozen sections of mouse lung cancer tissue and normal lung tissue (Scale bar: 100 μm). Data are shown as the Mean±SD; *p < 0.05; **p < 0.01; ***p < 0.001.

Finally, we sought to determine whether the observations in mice models could be verified in human lung adenocarcinoma tissues and the matched tumor-adjacent noncancerous lung tissues. We found a higher expression of SCD1 in CAFs than in NFs (Figures 6E and 6F). We further investigated the relationship between the expression level of SCD1 in fibroblasts and the clinical outcomes of lung adenocarcinoma patients using tissue microarrays ($n=75$). We found that high expression of SCD1 in fibroblasts was significantly associated with short overall survival among lung adenocarcinoma patients (Figure 6G). Consistent with the previous data [8], HIF-1 α was highly expressed in lung CAFs (α -SMA%+ cells) (Figures S4A and S4B). The Kaplan-Meier overall survival curves for the expression of HIF-1 α / α -SMA% in lung adenocarcinoma patients showed that the expression of HIF-1 α in fibroblasts was negatively correlated with the overall survival time (Figure 6H). Interestingly, we found that the expressions of SCD1 and HIF-1 α in fibroblasts were positively correlated (Figure 6I). Consistently, SCD1 was also highly expressed in mouse lung CAFs than in NFs (Figure 6J). These results demonstrated that the HIF-1 α /SCD1 axis in fibroblasts might affect lung cancer progression, and could be a potential therapeutic target in lung cancer.

Discussion

It is well-known that overgrowth of tumor cells restricts oxygen diffusion within the tumor, leading to insufficient blood supply to tumor cells and generating a hypoxic microenvironment, which in turn promotes the expression of HIF. HIF-1 α has been demonstrated the effectiveness at promoting the formation of tumor blood vessels [34] and tumor metastasis [35]. We have previously shown that HIF-1 α is essential for the activation of CAFs in lung cancer [8], and we showed here its ability to promote the accumulation of LDs in CAFs. HIF-1 α /SCD1 axis contributes to the accumulation of LDs. These results suggested that HIF-1 α can be targeted in lung cancer to block the activation of CAFs and provide insights into the mechanism of HIF-1 α -induced activation of CAFs.

Although the accumulation of LDs in fibroblasts has been investigated in cancers [36], little is known about the contribution of LDs to the function of fibroblasts in lung cancer. A recent study indicated that unsaturated fatty acids induced the immunosuppressive phenotype of TAMs and promoted tumor growth [19]. Kopecka et al. found that the expression and activity of multidrug efflux pumps were facilitated by lipids to modulate the multidrug resistance phenotype in cancer [37]. These findings

highlighted the complexity of the functions of LDs in different types of cells. In this study, we found that the increased LDs, especially the increased external intake or the synthesis of endogenous fatty acid in fibroblasts could elevate the expression of α -SMA and COL1A2, which indicated the activation of fibroblasts [38, 39]. When the formation of LDs was inhibited by the endogenous fatty acid blockers, the activated phenotype of fibroblasts was suppressed. Thus, based on our results, we concluded that the accumulation of LDs induced by the increased synthesis of fatty acids, plays an active role during the phenotypic transformation of fibroblasts. However, considering the heterogeneity of CAFs [2], we cannot yet determine whether there are subgroups of CAFs other than those with the high HIF-1 α phenotype that can promote the production of LDs. HIF-1 α is involved in the accumulation of LDs through different pathways [21]. Our previous work suggested that tumor-promoting fibroblasts could be activated by the upregulation of HIF-1 α , which was elevated by hypoxia, TGF- β or tumor CM [6]. In this study, we found that the upregulation of HIF-1 α promoted the accumulation of LDs in fibroblasts. Consistently, Parathath et al. reported that HIF-1 α induced the sterol synthesis and the suppression of cholesterol efflux to increase the sterol content in macrophages of atherosclerotic plaques [35].

As previously mentioned, SCD has a variety of isoforms that play different roles. Human adipose and liver tissues both exhibit significant levels of Scd1 expression. Scd1, Scd2, Scd3, Scd4, Scd5 were primarily expressed in adult mice. SCD5 was also present in chicken and mammals [40]. SCD1 is a central lipogenic enzyme that catalyzes the synthesis of monounsaturated fatty acids (MUFA) during lipogenesis in human [41], and it was significantly downregulated after the KO of HIF-1 α . SCD1 is known to play an essential role in the progression of cancers [42]. Gao et al. found that SCD1 promoted the stemness of ovarian cancer stem cells through the Hippo/YAP pathway [43]. Hence, SCD1 is a promising candidate for targeted drug development in STK11/KEAP1 co-mutant lung adenocarcinoma and ameliorated the drug resistance by inducing ferroptosis [44]. Wang et al. demonstrated that high expression of SCD1 was associated with the prognosis of gastric cancer patients and might be a therapeutic target in the treatment of gastric cancer [45]. SCD1 is also an important biomarker that can improve the survival of lung cancer stem cells, which are stabilized by EGFR to upregulate the synthesis of monounsaturated fatty acids and can promote the growth of lung cancer [46, 47]. However, the expression of SCD1 in lung cancer CAFs is still

unknown. In the present study, we found that HIF-1 α bound to the promoter of SCD1, which in turn promoted the production of lipid droplets in fibroblasts, and these results further established the importance of SCD1 in this process. Because of the differences between the cell lines, besides a reduction in the expression of SCD1, several other lipid catabolism genes like Acadm and Cpt-1 α were decreased in the MEF HIF-1 α -KO fibroblasts. Therefore, SCD1 is the main downstream gene of HIF-1 α that regulates the accumulation of LDs in fibroblasts. We cannot rule out the effects of other lipid metabolism-related genes, and this needs further evidence.

Moreover, we showed that the lung cancer patient survival time was negatively affected by the high expression of SCD1 in fibroblasts. The expression of HIF-1 α in lung CAFs was also negatively correlated with the survival time of lung cancer patients, which highlighted that the HIF-1 α /SCD1 axis in fibroblasts might be an ideal candidate for predicting the progression of lung cancer. Targeting SCD1 in lung cancer could significantly decrease the LDs in fibroblasts and restrain the formation of collagen in the TME.

Previous studies revealed that CAFs could enhance the production and delivery of ectosomes like lipids to cancer cells compared to that by NFs [48]. Moreover, several studies have confirmed the role of aberrant LD formation in promoting tumor cell survival in clear-cell renal cell carcinoma [49, 50] and showed a poor prognosis in high-grade serous carcinoma [51]. Our results suggested that the fibroblasts with more LDs were close to the tumor cells in the co-culture system. The number of LDs in tumor cells was elevated after the tumor cells were co-cultured with fibroblasts. It has been reported that the uptake of lipid metabolites secreted from CAFs by colorectal cancer (CRC) cells depends on the expression of CD36 [36]. However, in this study, the expression of CD36 in tumor cells did not differ between those co-cultured with fibroblasts and those that were not co-cultured with fibroblasts. We speculate that the cell-cell physical contact might be the main reason for the increased lipids in tumor cells that were co-cultured with fibroblasts. However, the detailed mechanism by which the lipid content increases in tumor cells needs further research.

In conclusion, our results established HIF-1 α as a master regulator of lipid metabolism in fibroblasts, elevating the abundance of LDs and leading to a tumor-promotion phenotype of lung fibroblasts. This signaling pathway is regulated by the HIF-1 α /SCD1 axis. Hence, the HIF-1 α /SCD1 axis represents a potential therapeutic target for lung cancer

management, along with other components of the lipid metabolism pathway. The findings may have important implications for the therapeutic targeting and development of prognostic markers for lung cancer.

Abbreviations

CAFs: Cancer associated fibroblasts; LDs: Lipid droplets; TME: Tumor microenvironment; NFs: Normal fibroblasts; iMEFs: Immortalized mouse embryonic fibroblasts; KO: Knock out; α -SMA: α -smooth muscle actin; HIF-1 α : Hypoxia inducible factor-1 α ; FAP: Fibroblast-activating protein; COL1A2: Collagen alpha-2(I) chain; PDPN: Podoplanin; FAS: Fatty acids; TAGs: Triglyceride; ADRP: Adipose differentiation-related protein; SCDs: Stearoyl CoA desaturases; BCAA: branched-chain amino acid; TGF- β 1: Transforming growth factor- β 1; PCNA: Proliferating cell nuclear antigen; CM: Conditioned medium; LLC: Lewis lung cancer cells; HRP: Horseradish-peroxidase-conjugated; RT-qPCR: Real-time quantitative polymerase chain reaction; DMEM: Dulbecco's modified eagle medium; Cocl2: Cobalt chloride; DGAT: Diglyceride acyltransferase; MAGL: Monoacylglycerol lipase.

Supplementary Material

Supplementary figures and tables.

<https://www.ijbs.com/v18p6114s1.pdf>

Acknowledgements

This work was supported by the National Natural Science Foundation of China (Grant Number: 82073231 and 81802281) and Sino-German Center Foundation (Grant Number: C-0072).

Author Contributions

Z.Q. and Y.Z. conceived and designed the experiments, revised the manuscript; Z.L., Z.G. and Y.B. revised the manuscript; Y.Z. performed most of experiments and prepared the first draft of the manuscript; J.W., X.L., S.L. Y.W. and F.W. performed parts of the experiments. All authors have read and approved the final manuscript.

Competing Interests

The authors have declared that no competing interest exists.

References

- Sung H, Ferlay J, Siegel RL, Laversanne M, Soerjomataram I, Jemal A, et al. Global cancer statistics 2020: GLOBOCAN estimates of incidence and mortality worldwide for 36 cancers in 185 countries. CA: a cancer journal for clinicians. 2021.
- Park D, Sahai E, Rullan A. SnapShot: Cancer-Associated Fibroblasts. Cell. 2020; 181: 486- e1.

3. Kobayashi H, Enomoto A, Woods SL, Burt AD, Takahashi M, Worthley DL. Cancer-associated fibroblasts in gastrointestinal cancer. *Nature reviews Gastroenterology & hepatology.* 2019; 16: 282-95.
4. Li J, Chen L, Qin Z. Multifaceted tumor stromal fibroblasts. *Cancer microenvironment: official journal of the International Cancer Microenvironment Society.* 2012; 5: 187-93.
5. Costa A, Kieffer Y, Scholer-Dahirel A, Pelon F, Bourachot B, Cardon M, et al. Fibroblast Heterogeneity and Immunosuppressive Environment in Human Breast Cancer. *Cancer cell.* 2018; 33: 463-79 e10.
6. Kalluri R. The biology and function of fibroblasts in cancer. *Nat Rev Cancer.* 2016; 16: 582-98.
7. Min KW, Kim DH, Noh YK, Son BK, Kwon MJ, Moon JY. Cancer-associated fibroblasts are associated with poor prognosis in solid type of lung adenocarcinoma in a machine learning analysis. *Scientific reports.* 2021; 11: 16779.
8. Zhang Y, Bian Y, Wang Y, Wang Y, Duan X, Han Y, et al. HIF-1alpha is necessary for activation and tumour-promotion effect of cancer-associated fibroblasts in lung cancer. *Journal of cellular and molecular medicine.* 2021; 25: 5457-69.
9. Sato R, Imamura K, Sembra T. TGF-β signaling activated by cancer-associated fibroblasts determines the histological signature of lung adenocarcinoma. 2021.
10. Wang L, Li X, Ren Y, Geng H, Zhang Q, Cao L, et al. Cancer-associated fibroblasts contribute to cisplatin resistance by modulating ANXA3 in lung cancer cells. *Cancer science.* 2019; 110: 1609-20.
11. Hutton C, Heider F, Blanco-Gomez A, Banyard A, Kononov A, Zhang X, et al. Single-cell analysis defines a pancreatic fibroblast lineage that supports anti-tumor immunity. *Cancer cell.* 2021; 39: 1227-44 e20.
12. Schworer S, Vardhana SA, Thompson CB. Cancer Metabolism Drives a Stromal Regenerative Response. *Cell metabolism.* 2019; 29: 576-91.
13. Sousa CM, Biancur DE, Wang X, Halbrook CJ, Sherman MH, Zhang L, et al. Pancreatic stellate cells support tumour metabolism through autophagic alanine secretion. *Nature.* 2016; 536: 479-83.
14. Mestre-Farrera A, Bruch-Oms M. Glutamine-Directed Migration of Cancer-Activated Fibroblasts Facilitates Epithelial Tumor Invasion. 2021; 81: 438-51.
15. Fiaschi T, Marini A, Giannoni E, Taddei ML, Gandellini P, De Donatis A, et al. Reciprocal metabolic reprogramming through lactate shuttle coordinately influences tumor-stroma interplay. *Cancer research.* 2012; 72: 5130-40.
16. Li Z, Sun C, Qin Z. Metabolic reprogramming of cancer-associated fibroblasts and its effect on cancer cell reprogramming. *Theranostics.* 2021; 11: 8322-36.
17. Becker LM, O'Connell JT, Vo AP, Cain MP, Tampe D, Bizarro L, et al. Epigenetic Reprogramming of Cancer-Associated Fibroblasts Dere regulates Glucose Metabolism and Facilitates Progression of Breast Cancer. *Cell reports.* 2020; 31: 107701.
18. Hershey BJ, Vazzana R, Joppi DL, Havas KM. Lipid Droplets Define a Sub-Population of Breast Cancer Stem Cells. *Journal of clinical medicine.* 2019; 9.
19. Wu H, Han Y, Rodriguez Sillke Y, Deng H, Siddiqui S, Treese C, et al. Lipid droplet-dependent fatty acid metabolism controls the immune suppressive phenotype of tumor-associated macrophages. *EMBO molecular medicine.* 2019; 11: e10698.
20. Bose D, Banerjee S, Chatterjee N, Das S, Saha M, Saha KD. Inhibition of TGF-beta induced lipid droplets switches M2 macrophages to M1 phenotype. *Toxicology in vitro: an international journal published in association with BIBRA.* 2019; 58: 207-14.
21. Wang H, Airola MV, Reue K. How lipid droplets "TAG" along: Glycerolipid synthetic enzymes and lipid storage. *Biochimica et biophysica acta Molecular and cell biology of lipids.* 2017; 1862: 1131-45.
22. Siniossoglou S. Phospholipid metabolism and nuclear function: roles of the lipid family of phosphatidic acid phosphatases. *Biochimica et biophysica acta.* 2013; 1831: 575-81.
23. Mylonis I, Simos G, Paraskeva E. Hypoxia-Inducible Factors and the Regulation of Lipid Metabolism. *Cells.* 2019; 8.
24. Masoud GN, Li W. HIF-1α pathway: role, regulation and intervention for cancer therapy. *Acta pharmaceutica Sinica B.* 2015; 5: 378-89.
25. Zheng F, Chen J, Zhang X, Wang Z, Chen J, Lin X, et al. The HIF-1α antisense long non-coding RNA drives a positive feedback loop of HIF-1α mediated transactivation and glycolysis. *Nature communications.* 2021; 12: 1341.
26. Huang Y, Lin D, Taniguchi CM. Hypoxia inducible factor (HIF) in the tumor microenvironment: friend or foe? *Science China Life sciences.* 2017; 60: 1114-24.
27. Politi K, Zakowski MF, Fan PD, Schonfeld EA, Pao W, Varmus HE. Lung adenocarcinomas induced in mice by mutant EGF receptors found in human lung cancers respond to a tyrosine kinase inhibitor or to down-regulation of the receptors. *Genes & development.* 2006; 20: 1496-510.
28. Wang Y, Zeng Y, Zhu L, Wan J, Lei N, Yao X, et al. Polysaccharides From Lentinus Edodes Inhibits Lymphangiogenesis via the Toll-Like Receptor 4/JNK Pathway of Cancer-Associated Fibroblasts. *Frontiers in oncology.* 2020; 10: 547683.
29. Zhang J, Chen L, Xiao M, Wang C, Qin Z, FSP1+ fibroblasts promote skin carcinogenesis by maintaining MCP-1-mediated macrophage infiltration and chronic inflammation. *The American journal of pathology.* 2011; 178: 382-90.
30. Deng WG, Jayachandran G, Wu G, Xu K, Roth JA, Ji L. Tumor-specific activation of human telomerase reverses transcriptase promoter activity by activating enhancer-binding protein-2beta in human lung cancer cells. *The Journal of biological chemistry.* 2007; 282: 26460-70.
31. Farago AF, Snyder EL, Jacks T. SnapShot: Lung cancer models. *Cell.* 2012; 149: 246- e1.
32. Dobrzyn P, Bednarski T, Dobrzyn A. Metabolic reprogramming of the heart through stearoyl-CoA desaturase. *Progress in lipid research.* 2015; 57: 1-12.
33. Furuhashi M, Hotamisligil GS. Fatty acid-binding proteins: role in metabolic diseases and potential as drug targets. *Nature reviews Drug discovery.* 2008; 7: 489-503.
34. Zhang C, Wang N, Tan HY, Guo W, Chen F, Zhong Z, et al. Direct inhibition of the TLR4/MyD88 pathway by geniposide suppresses HIF-1α-independent VEGF expression and angiogenesis in hepatocellular carcinoma. 2020; 177: 3240-57.
35. Zheng L, Wang B, Sun Y, Dai B. An Oxygen-Concentration-Controllable Multiorgan Microfluidic Platform for Studying Hypoxia-Induced Lung Cancer-Liver Metastasis and Screening Drugs. 2021; 6: 823-32.
36. Gong J, Lin Y, Zhang H, Liu C, Cheng Z, Yang X, et al. Reprogramming of lipid metabolism in cancer-associated fibroblasts potentiates migration of colorectal cancer cells. *Cell death & disease.* 2020; 11: 267.
37. Kopecka J, Trouillas P, Gasparovic AC, Gazzano E, Assaraf YG, Riganti C. Phospholipids and cholesterol: Inducers of cancer multidrug resistance and therapeutic targets. *Drug resistance updates: reviews and commentaries in antimicrobial and anticancer chemotherapy.* 2020; 49: 100670.
38. Özdemir BC, Pentcheva-Hoang T, Carstens JL, Zheng X, Wu CC, Simpson TR, et al. Depletion of carcinoma-associated fibroblasts and fibrosis induces immunosuppression and accelerates pancreas cancer with reduced survival. *Cancer cell.* 2014; 25: 719-34.
39. Sahai E, Astsaturov I, Cukierman E, DeNardo DG, Egeblad M, Evans RM, et al. A framework for advancing our understanding of cancer-associated fibroblasts. *Nature reviews Cancer.* 2020; 20: 174-86.
40. Wang Y, Botolin D, Xu J, Christian B, Mitchell E, Jayaprakasam B, et al. Regulation of hepatic fatty acid elongase and desaturase expression in diabetes and obesity. *Journal of lipid research.* 2006; 47: 2028-41.
41. AM AL, Syed DN, Ntambi JM. Insights into Stearoyl-CoA Desaturase-1 Regulation of Systemic Metabolism. *Trends in endocrinology and metabolism: TEM.* 2017; 28: 831-42.
42. Yu S, Lu Y, Su A, Chen J, Li J, Zhou B, et al. A CD10-OGP Membrane Peptolytic Signaling Axis in Fibroblasts Regulates Lipid Metabolism of Cancer Stem Cells via SCD1. *Advanced science.* 2021; 8: e2101848.
43. Gao Y, Li J, Xi H, Cui J, Zhang K, Zhang J, et al. Stearoyl-CoA-desaturase-1 regulates gastric cancer stem-like properties and promotes tumour metastasis via Hippo/YAP pathway. *British journal of cancer.* 2020; 122: 1837-47.
44. Wohlhieter CA, Richards AL, Uddin F, Hulton CH, Quintanal-Villalonga A, Martin A, et al. Concurrent Mutations in STK11 and KEAP1 Promote Ferroptosis Protection and SCD1 Dependence in Lung Cancer. *Cell reports.* 2020; 33: 108444.
45. Wang C, Shi M, Ji J, Cai Q, Zhao Q, Jiang J, et al. Stearoyl-CoA desaturase 1 (SCD1) facilitates the growth and anti-ferroptosis of gastric cancer cells and predicts poor prognosis of gastric cancer. *Aging.* 2020; 12: 15374-91.
46. Zhang J, Song F, Zhao X, Jiang H, Wu X, Wang B, et al. EGFR modulates monounsaturated fatty acid synthesis through phosphorylation of SCD1 in lung cancer. *Molecular cancer.* 2017; 16: 127.
47. Noto A, De Vitis C, Pisani ME, Roscilli G, Ricci G, Catizone A, et al. Stearoyl-CoA-desaturase 1 regulates lung cancer stemness via stabilization and nuclear localization of YAP/TAZ. *Oncogene.* 2017; 36: 4573-84.
48. Santi A, Caselli A, Ranaldi F, Paoli P, Mugnaioni C, Michelucci E, et al. Cancer associated fibroblasts transfer lipids and proteins to cancer cells through cargo vesicles supporting tumor growth. *Biochimica et biophysica acta.* 2015; 1853: 3211-23.
49. Gebhard RL, Clayman RV, Prigge WF, Figenhau R, Staley NA, Reesey C, et al. Abnormal cholesterol metabolism in renal clear cell carcinoma. *Journal of lipid research.* 1987; 28: 1177-84.

50. Qiu B, Ackerman D, Sanchez DJ, Li B, Ochocki JD, Grazioli A, et al. HIF2alpha-Dependent Lipid Storage Promotes Endoplasmic Reticulum Homeostasis in Clear-Cell Renal Cell Carcinoma. *Cancer discovery*. 2015; 5: 652-67.
51. Iwahashi N, Ikezaki M, Fujimoto M, Komohara Y, Fujiwara Y, Yamamoto M, et al. Lipid Droplet Accumulation Independently Predicts Poor Clinical Prognosis in High-Grade Serous Ovarian Carcinoma. *Cancers*. 2021; 13.